Design Using Finite Element Analysis of Switched Reluctance Motor for Electric Vehicle

Kazuhiro Ohyama [1], Kenichi Aso [2], Maged Naguib F. Nashed [3], Hiroaki Fujii [4], and Hitoshi Uehara [5]

[1] *Department of Electrical Engineering, Fukuoka Institute of Technology, ohyama@ee.fit.ac.jp*
[2] *Department of Electrical Engineering, Fukuoka Institute of Technology, mem04001@ws.ipc.fit.ac.jp*
[3] *Electronics Research Institutt, maged@eri.sci.eg*
[4] *Meiwa Manufacturing Co.,Ltd, h.fujii@meiwa-ss.co.jp*
[5] *Meiwa Manufacturing Co.,Ltd., h.uehara@meiwa-ss.co.jp*

Abstract

In this paper, Switched Reluctance Motor (SRM) for electric vehicle (EV) is designed using finite element method (FEM). The static torque of SRM is estimated with the magnetic field analysis. The temperature rise with time of SRM is estimated with the heat transfer analysis. First, the static torque and temperature rise with time of 600W SRM for sample machine are measured in the experiment, and they are compared with the calculated results using FEM under the same conditions. The validity of magnetic field analysis and heat transfer analysis is verified by the comparisons. Then, the 60 [kW] SRM for EV, which has the output characteristics equal to 1500 [cc] gasoline engine, is designed with the magnetic field analysis and heat transfer analysis.

Keywords

switched reluctance motor (SRM), electric vehicle (EV), design of SRM, and finite element method (FEM)

1. INTRODUCTION

Recently, the depletion problems of the petroleum energy, the serious environmental problem of global warming by CO_2 and air pollution by NO_x have been caused by the rapid development of the car society. As a solution for these problems, the following gradually spread: High mileage automobiles and low emissions vehicle represented in hybrid car (HV). However, especially, the penetration ratio of HV stagnates, and it is hard to be called a winning hit which solves the problem. As the reason, that the price of HV becomes higher than the price of gasoline-powered vehicle (GV) of the equal class is mentioned.

Switched reluctance motor (SRM) is a motor using reluctance torque which originates from the change of the magnetic resistance in magnetic circuit. The stator and rotor have the salient pole structure, and they are made from the laminated non oriented electrical steel. The concentrated winding coils are installed only in the stator. SRM has solid features and features as a low cost since SRM has the structure which is very simpler than induction motor and synchronous motor. And, winding coils and permanent magnet are not used in the rotor. Therefore, SRM has the possibility of standing high-speed rotations and operations in high temperature state, and the operations under inferior road surface condition for always receiving the impacts and vibration, which are assumed in the application to electric vehicle (EV) [Chiba, 2002].

The problems that torque pulsation and noise were big in the initial development of SRM drive existed. However, those problems are being solved by development of the power electronics and improvement in the technology [Morimoto et al., 1999]. The improvement of basic performance for the SRM drive contributes to the extension of the application field, and the application of SRM to the electric automobile (EV) begins to be examined recently. In the institutes, the following have already been observed: Reports on the design of SRM for EV and reports on performance enhancement of the control method for SRM assuming the application to EV.

Authors are tackling the project which develops the convert EV with the power performance which is equivalent to the GV of the 1500 [cc] class. In the project, SRM with solid features and features as a low cost is chosen, and SRM mounted in convert EV has been designed. The following goals as design guidelines are raised: Equivalent output characteristics with 1500cc gasoline engine, and making smaller and lighter. And, FF (the front engine front-wheel drive system) is adopted. Then, SRMs of 2 machines are used in order to omit the differential gear.

In this paper, design process of SRM for EV using mag-

netic field analysis and heat transfer analysis of finite element method (FEM) is reported. With the reference of authors, there seem to be no report which designed SRM for EV using both analysis of FEM. First, the static torque and temperature rise with time of 600W SRM for sample machine are measured in the experiment, and they are compared with the calculated results using FEM under the same conditions. The validity of magnetic field analysis and heat transfer analysis is verified by the comparisons. Then, the design procedure of SRM using both analysis is explained, and SRM for EV with output characteristics which is equivalent to 1500cc gasoline engine is designed.

2. STATIC TORQUE

2.1 Calculation of static torque

Inductance and static torque of 600W SRM for sample machine are calculated using ANSYS software of FEM. Figure 1 shows the analytical model of SRM. Table 1 shows the condition of analysis. Table 2 shows the specification of SRM. Using the analytical model as shown in Figure 1, the calculation is carried out by the two-dimensional static magnetic field analysis.

In this analysis, SRM used three-phase and which has stator of 6 poles and rotor of 4 poles. Since the pole number of the rotor is 4, the magnetic circuit becomes the same after rotating 90 degrees, when only one phase is excited. In addition, the stator salient pole and rotor salient pole repeat facing condition and non-facing condition for the interval of rotation 45 degrees. It is possible to obtain the inductance of the 360 degrees rotation by using the calculated inductance of the 45 degree rotations, if such geometric symmetry is utilized. Then, non-facing condition of stator salient pole and rotor salient pole is defined as 0 degrees, and the rotor is made to rotate 45 degrees of the facing condition. For each 1 degree, the inductance and static torque of one phase are calculated.

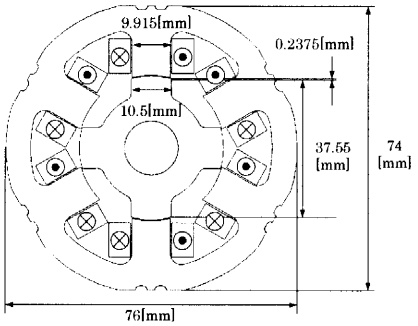

Fig. 1 Analytical model

Table 1 Condition of analysis

number of node	15173
number of element	7636
mesh size (all area)	0.0013
shape of element	triangle
excitation phase of coil	one phase only
excitation current	10.0 [A]
current density	1.559×10^6 [A/m^2]
partial area of coil	51.3 [mm^2]
analysis range	0~45 [deg]

Table 2 Specification of SRM

stator outer diameter	76 [mm]
rotor outer diameter	37.55 [mm]
output	600 [W]
air gap	0.2375 [mm]
stack length	50 [mm]
number of windings/pole	20 [turns/pole]
stator/rotor poles	6/4

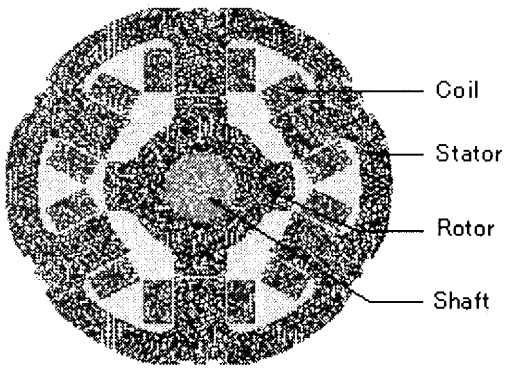

Fig. 2 Element distribution

At rotor position θ, the magnetic co energy $W'(\theta)$ is calculated according to the following equation, while the rotor is made to rotate from 0 degrees to 45 degrees for each 1 degree.

$$W'(\theta) = \frac{1}{2}\sum_i \frac{B_i^2}{\mu_i} v_i \qquad (1)$$

Where B_i is the magnetic flux density of each element, μ_i is the permeability of each element, and v_i is the volume of each element.

Inductance $L(\theta)$ in rotor position θ is calculated according to the following equation.

$$L(\theta) = \frac{2W'(\theta)}{i^2} \qquad (2)$$

Where i is the excitation current.

Figure 3 shows the inductance $L(\theta)$ in rotor position θ calculated using equations (1) and (2).

Using the $W'(\theta)$ or $L(\theta)$, the reluctance torque $T(\theta)$ is calculated according to the following equation.

$$T(\theta) = \frac{\partial W'(\theta)}{\partial \theta} = \frac{1}{2} i^2 \frac{dL(\theta)}{d\theta} \qquad (3)$$

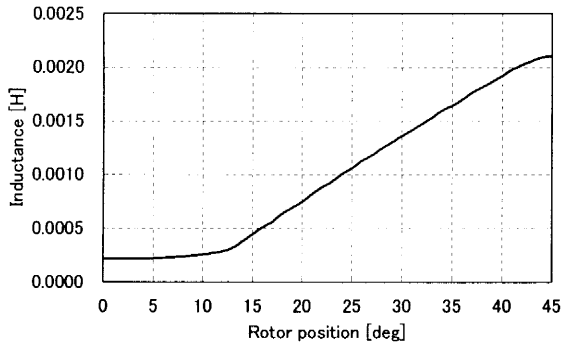

Fig. 3 Calculated results of inductance

Figure 4 shows static torque $T(\theta)$ in rotor position θ calculated using equation (3). $T(\theta)$ of the positive direction is obtained regardless of the current direction, if the exciting current is flowing when $L(\theta)$ increases, because $T(\theta)$ is proportional to the derivative for the rotor position of the inductance. In short, the rotor keeps rotating in the positive direction, because the torque of the positive direction is obtained at every excitation, when the winding is continued to be excited in the position where the gradient of $L(\theta)$ becomes a positive direction.

Fig. 4 Calculated results of static torque

2.2 Experimental results

The static torque in exciting only one phase was measured using 600W SRM of sample machine. Figure 5 shows the experiment circuit. The excitation current of

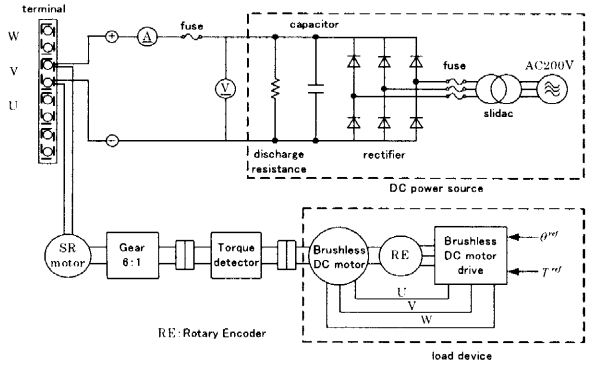

Fig. 5 Experiment circuit

4 [A] is applied to the one phase of SRM using the DC power source, and static torque at rotor position θ was measured using the torque meter. The rotor position of SRM was fixed using the brushless DC motor drive. The rotor position of SRM can be fixed by controlling rotor position of the brushless DC motor using the brushless DC motor drive. There is a speed reducer between brushless DC motor and SRM. The gear ratio is 6:1. Therefore, it is possible to rotate the SRM for 1 degree by giving the command signal which rotates 1/6 degrees to the brushless DC motor drive. And, the static torque in the position fixed by the brushless DC motor drive can be measured using the torque meter. The comparison of calculated and experimental results of the static torque is shown in Figure 6. The static torque calculated using magnetic field analysis agrees well with the experimental result measured in same condition. Therefore, the validity of the magnetic field analysis using FEM utilized for the design was proven.

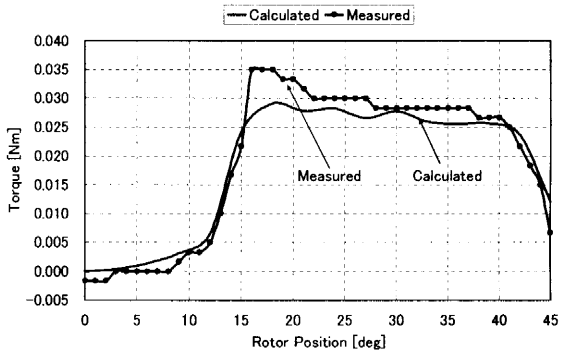

Fig. 6 Comparison of calculated results and experimental results of Static torque

3. HEAT TRANSFER ANALYSIS

3.1 Calculation of temperature rise

Heat transfer analysis is carried out using the analytical model shown in Figure 1. However, in the actual analytical model used, in order to choose the condition equal to that of experiment, the rotor was removed, and its region was changed in air space, and number of turns of the coil was changed at 8 [turn]. Number of turns of the coil was changed, because the stator in the laboratory was 8 [turn].

The heat quantity of the coil must be proven in order to carry out the heat transfer analysis. Then, the magnetic field analysis is carried out in order to obtain the heat quantity of the coil. In the magnetic field analysis, the voltage drop load is given to the coils of excitation phase, and the Joule heat per unit cube product of the coil is calculated. The Joule heat obtained in the magnetic field analysis is set at the coils, and the heat transfer analysis is carried out.

The heat transfer between SRM and outside air is done by natural convection. The heat transfer coefficient in natural convection was obtained from the simple formula for heat transfer of natural convection [Tanishita, 1986]. In the stator surface of which contacting plane with the air is smooth, the simple formula for the laminar flow shown in following equation is used.

$$\alpha = 1.42 \times (\frac{\Delta t}{l})^{\frac{1}{4}} \quad (4)$$

Where, α is a heat transfer coefficient, Δt is a gradient of temperature change, and l is the core thickness. And, the simple formula for the turbulent flow shown in following equation is used in the coil surface of which the plane which contacts the air is not smooth.

$$\alpha = 0.95 \times (\Delta t)^{\frac{1}{3}} \quad (5)$$

Temperature gradient Δt used in equations (4) and (5) is assumed its initial value to be 0 [K]. The α is calculated for the fixed time, and it is renewed in point of time in which temperature gradient occurred in boundary surface. In this analysis, it was renewed in the 5 minutes interval by 60 minutes of which the temperature rise was big. And, it was renewed in the 20 minute interval after 60 minutes that it approached the steady state and that the temperature change decreases.

Figure 7 shows the temperature distribution after 120 minutes in applying 10 [A] of only one phase. Figure 8 shows the temperature rise in coil and stator during 120 minutes. The positions where the temperature rise of

Table 3 Material property

Material	Temperature [°C]	Density [kg/m³]	Specific Heat [J/Kg·K]	Termal Conductivity [W/m·K]
Coil(Copper)	20	8950	0.383×10^3	386
	100		0.398×10^3	379
	300		0.425×10^3	369
Silicon Steal	20	7770	0.460×10^3	42
Air (1atm,300K)	27	1.1763	1.007×10^3	0.02614

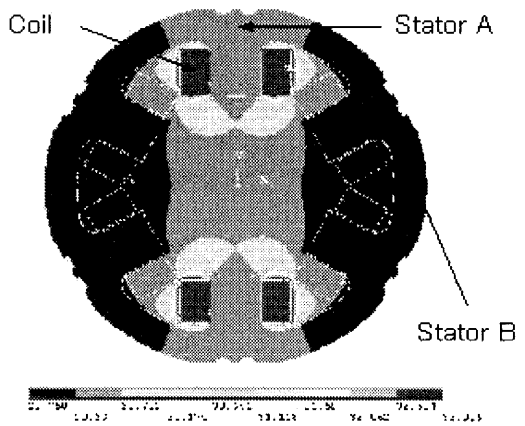

Fig. 7 Temperature distribution after 120 minutes

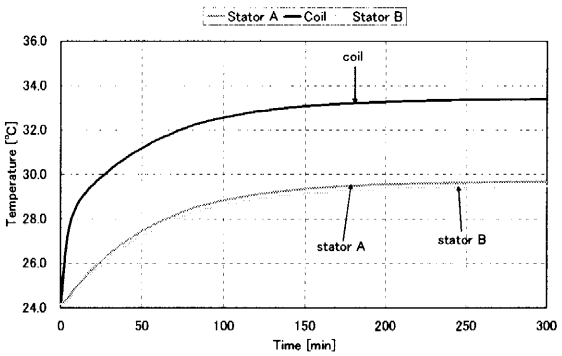

Fig. 8 Calculated results of temperature rise

Figure 8 is observed are 3 places shown in Figure 7. The one place is coil surface of the excited phase, and the other 2 places are the stator surface. Stator A is stator surface of the base of the stator salient pole division of the excited phase. And, stator B is stator surface which has separated from the excitation phase most.

3.2 Experimental results

Using the stator of SRM for sample machine as well as the heat transfer analysis in 3.1, the temperature change of the coil and stator in exciting only one phase was measured. The excitation current of 10 [A], which was the same condition with the heat transfer analysis, was applied. Using the radiation thermometer, the temperature of the coil and stator was measured in every 1 minute. The emissivity of the radiation thermometer was made to be 0.86. The room temperature in the experiment was 24.2 [degree centigrade]. Figure 9 shows the comparison of experimental results and calculated results of temperature rise. The continuous line is calculated result, and the plotting is the experimental result. The thermometry was carried out at the 3 places equal to those of the heat transfer analysis.

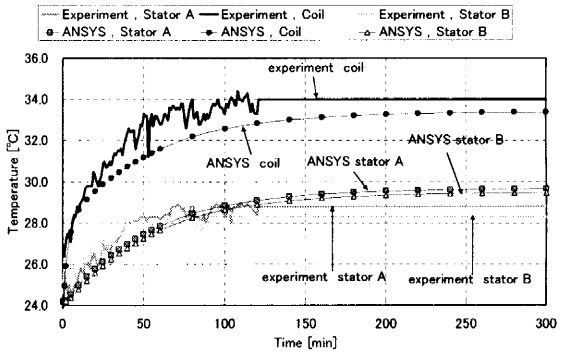

Fig. 9 Comparison of experimental results and calculated results of temperature rise

The experimental results and calculated results have reached an equilibrium state in about 120 minutes, as it is shown in Figure 9. The calculated results have low-

ered only about 1.0 [degree centigrade] further than the experimental result on the temperature of coil. The experimental results rises only about 1.0 [degree centigrade] further than the calculated results on the temperature of stator. The calculated results of temperature rise of the coil in heat transfer analysis tended to decrease further than experimental result. The heat transfer analysis using FEM has produced the error for the experimental result. However, the sufficient accuracy which can be used for the design can be ensured by considering the safety factor. Then, the heat transfer analysis of SRM for EV is carried out using fixed value ($\alpha = 1.0$) of which safety factor is considered.

4. DESIGN OF SRM FOR EV

4.1 Dimension of SRM and moderating ratio

Considering the space in engine room of the base car, the stator diameters of 250, 300, and 350 [mm] are made to be candidates, and the stator depths of 150, 200, and 250 [mm] are examined for each diameters. The shape of rotor and stator was decided by referencing [Miller, 1993]. Figure 10 shows analytical model for stator diameter of 350 [mm]. Table 4 shows condition of analysis. Table 5 shows the specification of SRM. An output of SRM is designed at 60 [kW] in order to obtain output characteristics equal to gasoline engine of the 1500cc class. Assuming the utilization of 2 SRMs in order to omit the differential gear, the SRM of 30 [kW] is designed.

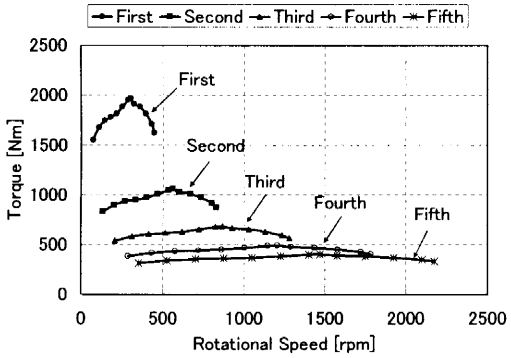

Fig. 10 Engine performance curve of gasoline vehicle

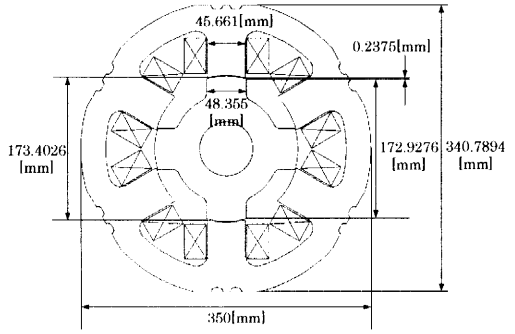

Fig. 11 Analytical model for stator diameter of 350 (mm)

Table 4 Condition of analysis

stator outer diameter	250 [mm]	300 [mm]	350 [mm]
number of node	11377～11785	11481～11849	11945～12633
number of element	5598～5802	5650～5834	5866～6210
mesh size (all area)	0.0055	0.0065	0.0070
shape of element	triangle	triangle	triangle
excitation phase of coil	one phase only	one phase only	one phase only
excitation current	100 [A]	100 [A]	100 [A]
current dencity	8.4669×10^6 [A/m²]	8.3819×10^6 [A/m²]	8.4560×10^6 [A/m²]
partial area of coil	555.10 [mm²]	799.34 [mm²]	1087.99[mm²]
analysys range	0～45 [deg]	0～45 [deg]	0～45 [deg]

Table 5 Specification of SRM

stator outer diameter	250 [mm]	300 [mm]	350 [mm]
rotor outer diameter	123.5197 [mm]	148.2236 [mm]	172.9276 [mm]
output	30 [KW]×2	30 [KW]×2	30 [KW]×2
air gap	0.2375 [mm]	0.2375 [mm]	0.2375 [mm]
stack length	150, 200, 250 [mm]	150, 200, 250 [mm]	150, 200, 250 [mm]
number of windings/pole	47 [turns/pole]	67 [turns/pole]	92 [turns/pole]
stator/rotor poles	6/4	6/4	6/4

Table 6 Average torque

Motor size [cm]	stack length [cm]	Excitation Current [A]	3 phase Average Torque [Nm]
25	15	100	148.45123
	20	100	197.93497
	25	100	247.41871
30	15	100	238.94170
	20	100	318.58893
	25	100	398.23616
35	15	100	356.26735
	20	100	475.02313
	25	100	593.77892

Table 7 Average torque considering moderating ratio

Motor size [cm]	stack length [cm]	Excitation Current [A]	3 phase Average Torque [Nm]
25	15	100	742.25613
	20	100	989.67484
	25	100	1237.09356
30	15	100	1194.70848
	20	100	1592.94464
	25	100	1991.18080
35	15	100	1781.33675
	20	100	2375.11567
	25	100	2968.89458

Large torque is required so that the EV may start. Table 6 shows the average torque of sum total of 2 SRMs designed. The average torque is the sum total of the three-phase. The average torque in not using speed reducer shown in Tables 6 is much smaller than the performance curve of gasoline engine shown in Figure 10. From this fact, it is clear that speed reducer is necessary. Then, the speed reducer shall be established between the SRM and driving shafts. The speed reducer used here is only one ratio, and it is not a change gear used in gasoline vehicles (GV).

Though, it is good for the acceleration from the arrest state, because the torque increases, when moderating ratio is increased, and the maximum speed lowers. And, the dimension of the gearbox increases, and it does not fit the space in the engine room. Then, optimum moderating ratio of 1/5 is adopted, and starting torque and

performance of high speed operation which are equivalent to GV are obtained. Table 7 shows the average torque of sum total of 2 SRMs considering moderating ratio of 1/5. The average torques which are equivalent to the peak torque of GV are obtained for the following conditions: the depth of 250 [mm] for diameter of 300 [mm], and the depths of 200 and 250 [mm] for the for the diameter of 350 [mm]. Considering the shape of the space in engine room of the base car, there is no allowances for the depth. Then, diameters of 350 [mm] and depth of 200 [mm] are selected.

Only static torque which arises, when the constant current has been applied in the arrest state, has been examined until now. However, the generated torque decreases, because the delay occurs in the stator current, when the rotational frequency of SRM rises. Dynamic simulation considering the electrical characteristic of the coil and mechanical system are necessary to examine the generated torque in the general transit. The generated torque in the general transit-time will be examined in the next project.

4.2 Calculation of temperature rise

The temperature rise of SRM for continuous operation at the rated current of 100 [A] is verified. In the rated operation, the temperature of the coil is forbidden to become over 140 [degree centigrade]. Then, the heat transfer analysis in applying current of 100 [A] to the coil for 1 hour is carried out, and the temperature rise of coil and stator is verified.

The analysis was carried out using the analytical model which added cooling system to analytical model of Figure 11. Figure 12 shows the element distribution of the analytical model which added cooling system. The analysis was carried out using the copper pipe using the water as a cooling system as a refrigerant. The copper pipe was used as a cooling system, and the water was used as a refrigerant. The shape of the copper pipe is the column of the 14 [mm] outer diameter and 12 [mm] inner diameter.

The initial temperature difference is made to be 0, the calculation is started, as it was described at 3.1, and heat transfer coefficient α is renewed in point of time in which temperature gradient arose. However, the constant value $\alpha = 1.0$ [W/m^{2}K] considering the safety factor is used for the stator surface in this analysis, since the calculation time is shortened. In comparison with the case in which it is calculated while α is renewed considering temperature change, the temperature rise increases when it is calculated using constant value $\alpha = 1.0$ [W/m^{2}K]. The water is compulsorily run in the copper pipe. Therefore, it is the forced convection of the water in the copper pipe. The general value of average heat transfer coefficient for the water flow inside the cylinder is 6000 [W/m^{2}K] [Nishikawa et al., 1982]. Then, $\alpha = 6000$ [W/m^{2}K] is set for the water in the copper pipe in this analysis. The air gap in the SRM inside becomes aerial forced convection, because the rotor rotates. The average heat transfer coefficient of the aerial forced convection in the cylinder is 50 [W/m^{2}K] [17]. However, the SRM inside is hard to be called a cylinder. Then, the heat transfer coefficient of the SRM inside is 30 [W/m^{2}K], which is middle value of the average heat transfer coefficient 6 [W/m^{2}K] of natural convection and average heat transfer coefficient 50 [W/m^{2}K] of forced convection.

Table 8 Material property

Material	Temperature [°C]	Density [kg/m^3]	Specific Heat [J/Kg·K]	Termal Conductivity [W/m·K]
Coil·copper pipe (Copper)	20	8950	0.383×10^3	386
	100		0.398×10^3	379
	300		0.425×10^3	369
Silicon Steal	20	7770	0.460×10^3	42
Iron	20	7830	0.465×10^3	54
Water	20	998.2	4.183×10^3	0.602
Air (1atm,300K)	27	1.1763	1.007×10^3	0.02614

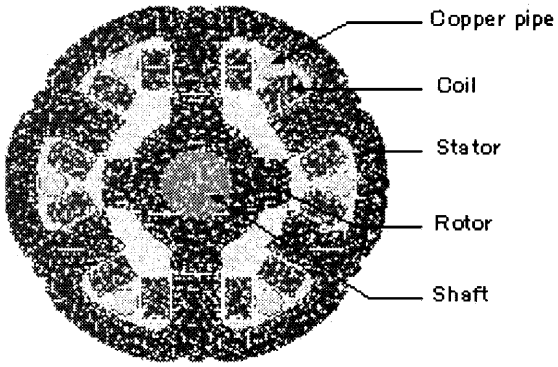

Fig. 12 Element distribution

The current is applied to each coil in the order of the excitation timing. It is assumed that the three-phase current is flowing simultaneously, because the excited phase is switched at high speed. The current of 100 [A] per 1 phase is flowing instantaneously. However, it is assumed that it is flowing at the 57.74 [A] per 1 phase is flowing, because it is assumed that the current of three-phase is flowing simultaneously.

Figure 13 shows the temperature distribution. The temperature after 60 minutes is 62.2 [degree centigrade]. And, it can be confirmed that the temperature has reached an equilibrium state from Figure 14. The temperature of the coil does not exceed 140 [degree centigrade] which is an allowable temperature, even if the rated current of 100 [A] is applied for 1 hour. Therefore, it can be confirmed that the coil can resist a heat sufficiently, even if the rated continuous operation is carried out.

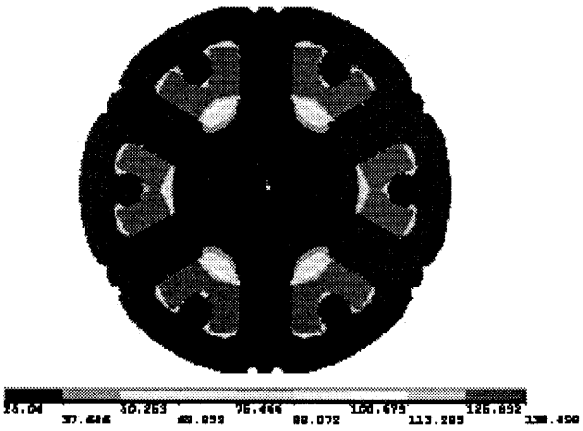

Fig. 13 Temperature distribution

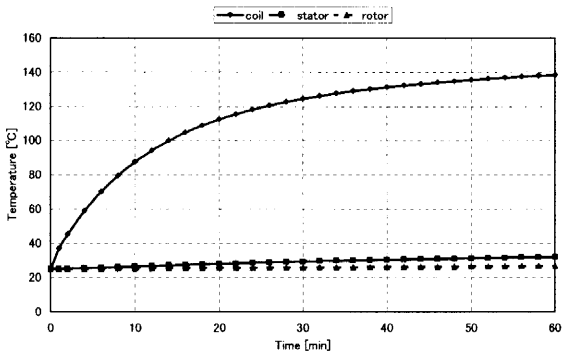

Fig. 14 Temperature rise for 30kW rated operation

5. CONCLUSION

It was confirmed that static torque calculated in magnetic field analysis and temperature rise calculated in heat transfer analysis agreed with the experimental results well. Therefore, it was confirmed that magnetic field analysis and heat transfer analysis using FEM could be utilized for the design of SRM.

The SRM for EV, of which output characteristics equal to output characteristics of GV of the 1500cc class, was designed. And, the heat transfer analysis was carried out for the continuous rating operation. It was confirmed that the temperature of coil does not exceed 140 [degree centigrade] which is an allowable temperature of the coil.

References

Cai, W., P. Pillay, Z. Tang, and A. M. Omekanda, Low-Vibration Design of Switched Reluctance Motors for Vehicle Propulsion Using Model Analysis, *IEEE Trans. Ind. Applicat.*, Vol. 39, 971-977, 2003.

Chiba, A., Design of a Switched Reluctance Drive and Its Application, *J. of Magn. Soc. Japan*, Vol. 26, No. 8, 909-914, 2002.

Goto, H., T. Watanabe, H. Guo, A. Honda, and O. Ichinokura, Development of an Electric Vehicle with Outer Rotor Type Multipolar Switched Reluctance Motors, *IEE Japan*, RM-04-54, 2004.

Inderka, R. B., and R. W. A. A. D. Doncker, High-Dynamic Direct Average Torque Control for Switched Reluctance Drives, *IEEE Trans. Ind. Applicat.*, Vol. 39, 1040-1045, 2003.

Inderka, R. B., M. Menne, and R. W. A. A. D. Doncker, Control of Switched Reluctance Drives for Electric Vehicle Application, *IEEE Trans. Ind. Electron.*, Vol. 49, 48-53, 2002.

Inamura, S., and K. Sawa, A Study on Temperature Analysis of Switched Reluctance Motor, *IEEJ Trans. IA*, Vol. 123, No. 4, 422-428, 2003.

Miller, T. J. E. , *Switched Reluctance Motors and Their Control*, Clarendon Press, 1993.

Morimoto, M., N. Matsui, and Y. Takeda, Recent Advances of Reluctance Motors, *IEEJ Trans. IA*, Vol. 119, No. 10, 1145-1148, 1999.

Nishikawa, and Fujita, *Mechanical Engineering Basic Lecture. Heat Transfer Engineering*, Rikogakusha Publishing, 81-82, 1982.

Omekanda, M., A New Technique for Multidimensional Optimization of Switched Reluctance Motors for Vehicle Propulsion, *IEEE Trans. Ind. Applicat.*, Vol. 39, 672-676, 2003.

Rahman, K. M., and S. E. Schulz, Design of High-Efficiency and High-Torque-Density Switched Reluctance Motor for Vehicle Propulsion, *IEEE Trans. Ind. Applicat.*, Vol. 38, 1500-1507, 2002.

Rahman, K. M., and S. E. Schulz, High-Performance Fully Digital Switched Reluctance Motor Controller for Vehicle Propulsion, *IEEE Trans. Ind. Applicat.*, Vol. 38, 1062-1071, 2002.

Rahman, K. M., B. Fahimi, G. Suresh, A. V. Rajarathnam, and M. Ehsani, Application of Switched Reluctance Motor Application to EV and HEV: Design and Control Issues, *IEEE Trans. Ind. Applicat.*, Vol. 36, 111-121, 2000.

Ramamurthy, S. S., and J. B. Balda, Sizing a Switched Reluctance Motor for Electric Vehicles, *IEEE Trans. Ind. Applicat.*, Vol. 37, 1256-1264, 2001.

Schulz, S. E., and K. M. Rahman, High-Performance Digital PI Current Regulator for EV Switched Reluctance Motor Drives, *IEEE Trans. Ind. Applicat.*, Vol. 39, 1118-1126, 2003.

Suzuki, Y., K. Nakamura, and O. Ichinokura, Consideration on Multipolar Switched Reluctance Motors, *IEE Japan*, RM-03-87, 1-6, 2003.

Tanishita, *Heat Transfer Engineering*, Shokabo Publishing, 155-176, 1986.

Wang, S., Q. Zhan, Z. Ma, and L. Zhou, Implementation of a 50-kW Four-Phase Switched Reluctance Motor Drive System for Hybrid Electric Vehicle, *IEEE*

Trans. Magn., Vol. 41, 501-504, 2005.

(Received November 30, 2005; accepted December 20, 2005)